J Bioenerg Biomembr (2010) 42:99–109
DOI 10.1007/s10863-010-9280-0

Probing the effect of transport inhibitors on the conformation of the mitochondrial citrate transport protein via a site-directed spin labeling approach

June A. Mayor · Jiakang Sun · Rusudan Kotaria · D. Eric Walters · Kyoung Joon Oh · Ronald S. Kaplan

Received: 2 February 2010 / Accepted: 22 February 2010 / Published online: 31 March 2010

Abstract The present investigation utilized the site-directed spin labeling method of electron paramagnetic resonance (EPR) spectroscopy to identify the effect of citrate, the natural ligand, and transport inhibitors on the conformation of the yeast mitochondrial citrate transport protein (CTP) reconstituted in liposomal vesicles. Spin label was placed at six different locations within the CTP in order to monitor conformational changes that occurred near each of the transporter's two substrate binding sites, as well as at more distant domains within the CTP architecture. We observed that citrate caused little change in the EPR spectra. In contrast the transport inhibitors 1,2,3-benzenetricarboxylate (BTC), pyridoxal 5′-phosphate (PLP), and compound 792949 resulted in spectral changes that indicated a decrease in the flexibility of the attached spin label at each of the six locations tested. The rank order of the immobilizing effect was compound 792949 > PLP > BTC. The four spin-label locations that report on the CTP substrate binding sites displayed the greatest changes in the EPR spectra upon addition of inhibitor. Furthermore, we found that when compound 792949 was added vectorially (i.e., extra- and/or intra-liposomally), the immobilizing effect was mediated nearly exclusively by external reagent. In contrast, upon addition of PLP vectorially, the effect was mediated to a similar extent from both the external and the internal compartments. In combination our data indicate that: i) citrate binding to the CTP substrate binding sites does not alter side-chain and/or backbone mobility in a global manner and is consistent with our expectation that both in the absence and presence of substrate the CTP displays the flexibility required of a membrane transporter; and ii) binding of each of the transport inhibitors tested locked multiple CTP domains into more rigid conformations, thereby exhibiting long-range inter-domain conformational communication. The differential vectorial effects of compound 792949 and PLP are discussed in the context of the CTP homology-modeled structure and potential mechanistic molecular explanations are given.

Keywords Citrate transporter · Liposomes · Mitochondria · Membrane proteins · Site-directed spin labeling · Electron paramagnetic resonance · Inhibitors

Abbreviations

BTC	1,2,3-benzenetricarboxylate
CTP	citrate transport protein
EPR	electron paramagnetic resonance
MTSSL	(1-oxyl-2,2,5,5-tetramethyl-Δ^3-pyrroline-3-methyl) methanethiosulfonate
PLP	pyridoxal 5′-phosphate
RMS	root-mean-square
sarkosyl	sodium N-lauroylsarcosinate
TMD	transmembrane domain

Introduction

The mitochondrial citrate transport protein (CTP) catalyzes the movement of citrate across the inner membrane. In higher

June A. Mayor and Jiakang Sun contributed equally to this work.

J. A. Mayor · J. Sun · R. Kotaria · D. E. Walters · K. J. Oh (✉) · R. S. Kaplan (✉)
Department of Biochemistry & Molecular Biology,
Rosalind Franklin University of Medicine and Science,
The Chicago Medical School,
3333 Green Bay Road,
North Chicago, IL 60064, USA
e-mail: kyoung.oh@rosalindfranklin.edu
e-mail: ronald.kaplan@rosalindfranklin.edu

eukaryotic organisms the CTP primarily catalyzes citrate efflux that is obligatorily linked to the influx of either another tricarboxylate (e.g., isocitrate), a dicarboxylate (malate), or phosphoenolpyruvate (Robinson et al. 1971; Palmieri et al. 1972). In yeast the CTP is thought to primarily catalyze citrate efflux in exchange for isocitrate influx. Upon reaching the intermembrane space, citrate passively diffuses through the outer mitochondrial membrane's voltage-dependent anion selective channel in order to reach the cytoplasm. Once in the cytoplasm, citrate serves as a key carbon source which supports fatty acid, triacylglycerol, and sterol biosyntheses (Watson and Lowenstein 1970; Brunengraber and Lowenstein 1973; Endemann et al. 1982; Conover 1987). Thus, clearly the CTP is essential to the energy metabolism of many eukaryotic cell types. Moreover, the altered function of this transporter in certain disease states (e.g., diabetes (Kaplan et al. 1990b), cancer (Kaplan et al. 1982), and possibly DiGeorge Syndrome (DGS) (Heisterkamp et al. 1995)) likely plays an important role in the aberrant bioenergetics that characterizes these pathologies. With regard to diabetes, a recent study showed that citrate efflux from mitochondria on the CTP plays an essential role in controlling glucose-stimulated insulin secretion (GSIS) from pancreatic islet β-cells (Joseph et al. 2006). Suppression of CTP function, either by pharmacologic use of BTC, or by siRNA-mediated suppression of CTP expression, resulted in potent inhibition of GSIS, whereas enhancement of CTP expression caused stimulation. Therefore, the CTP may be essential to the regulation of insulin secretion from pancreatic β-cells (Joseph et al. 2006; Jensen et al. 2008).

In view of the prominent role that the CTP plays in physiology and pathology, we have conducted extensive investigations with the aim of understanding its structure-based mechanism. These studies include purifying the reconstitutively active form of the rat liver mitochondrial CTP (Kaplan et al. 1990a), followed by the cloning (Kaplan et al. 1993) and overexpression of this carrier from both rat liver (Xu et al. 1995) and yeast (Kaplan et al. 1995). Subsequently, we developed a homology-modeled structure of the CTP (Walters and Kaplan 2004) using the x-ray structure of the mitochondrial ADP/ATP carrier as a guide (Pebay-Peyroula et al. 2003). Interpretation of chemical modification ± substrate protection data obtained with site specific mutants (Kaplan et al. 2000a; Ma et al. 2004, 2005), within the framework of the CTP homology model has resulted in the identification of substantial portions of the substrate translocation pathway. Moreover, kinetic analysis of single-Cys CTP mutants in combination with molecular modeling using our homology-modeled structure has: *i)* resulted in the identification of two substrate binding sites per CTP monomer that reside at increasing depths within the bilayer (Ma et al. 2007); and *ii)* enabled characterization of the inhibition mechanism of BTC, the classical inhibitor of the CTP, as well as of PLP, a lysine-selective reagent (Remani et al. 2008). Recently, *in silico* screening of the ZINC database of commercially available compounds, followed by experimental testing of selected compounds, led to the discovery of the first purely competitive inhibitor of the CTP (i.e., compound 792949) (Aluvila et al. 2010). Docking calculations indicate that this inhibitor likely spans and binds simultaneously to CTP binding sites 1 and 2 (Aluvila et al. 2010).

In order to further advance our understanding of the translocation mechanism of the CTP, we used EPR spectroscopy in conjunction with site-directed spin labeling (Hubbell et al. 1998, 2000; Feix and Klug 1998; Columbus and Hubbell 2002; Klug and Feix 2008; Klare and Steinhoff 2009) of single-Cys CTP mutants in order to probe the effect of substrate and inhibitors on conformational change. Sites were chosen for labeling to probe conformational changes near the two substrate binding sites within the CTP, as well as a matrix-facing loop and possibly the monomer-monomer interface in homodimeric CTP. We observed that: i) citrate caused little change in the EPR spectra of spin-label introduced at the above six locations; ii) three CTP inhibitors, BTC, compound 792949, and PLP caused significant spectral changes that imply reduced flexibility of the spin label at each location; the rank order of inhibition was 792949 > PLP > BTC; and iii) the immobilizing effect of compound 792949 was mediated almost exclusively by addition of external reagent, whereas with PLP both external and internal reagent were required. In combination, these studies have resulted in the discovery of inhibitors that lock the CTP into an immobilized conformation(s), which may represent one or more of the conformations that CTP assumes during its transport cycle. Furthermore, they demonstrate that conformational communication exists between distant domains within this transporter. The mechanistic implications of these studies are discussed.

Experimental procedures

Overexpression and Purification of Single-Cys CTP Mutants Single-Cys CTP mutants were constructed utilizing the Strategene QuikChange mutagenesis kit with the Cys-less CTP gene in pET-21a(+) serving as the starting template as previously described (Xu et al. 2000; Ma et al. 2004). Each CTP variant was overexpressed in *E. coli* and the inclusion body fraction was isolated (Kaplan et al. 1995; Xu et al. 1995). Mutant CTPs were extracted from inclusion bodies with 1.2% sarkosyl, ultracentrifuged, and stored at −80°C. Each mutant then was purified as follows (Kaplan et al. 2000b): 1) Thawed inclusion body extract (9–9.5 mg) was

adsorbed to a MonoQ HR 5/5 column equilibrated with Buffer A (10 mM Tris-HCl, pH 7.6; 0.3% sarkosyl, 1 mM DTE). 2) The column was sequentially washed in Buffer A, then in Buffer A + 460 mM NaCl. 3) CTP was eluted in a shallow gradient of Buffer A + 460–550 mM NaCl. 4) The eluate was analyzed by SDS-PAGE and the most highly purified fractions were combined with two or three other MonoQ-purified eluates of the same mutant. Combined MonoQ preparations of a single-Cys CTP mutant were applied to a Sephacryl S-300 (26/60) column equilibrated in Buffer B (10 mM Tris-HCl, pH 7.6; 150 mM NaCl, 0.3% sarkosyl, 1 mM DTE). The CTP eluted in a single symmetrical peak with an elution volume of approximately 156 mL, was concentrated, and stored at −80°C.

Spin Labeling of CTP Mutants Purified single-Cys CTP mutants (~80 nmol) were desalted twice using Micro Bio-Spin Columns (BioRad) that had been equilibrated in Buffer C (30 mM Hepes, 12.5 mM NaCl, 0.25 mM EDTA, 0.3% sarkosyl, pH 7.14). The desalted CTP mutants were incubated with a 10-fold molar excess of spin label I (Berliner et al. 1982) to generate side-chain R1 as shown in Fig. 1. The labeling reaction was conducted for 5 h at room temperature in the dark with gentle mixing every hour. Each labeled reaction mix was desalted three times on Bio-Spin columns before the CTP was incorporated into phospholipid vesicles via the freeze-thaw-sonication technique as previously described (Kaplan et al. 1990a, b, 1995). Following the thawing and probe sonication steps, the spin labeled proteoliposomes were chromatographed on Dowex in Buffer D (120 mM Hepes, 50 mM NaCl, 1 mM EDTA, pH 6.9), diluted with Buffer D (pH 7.1), and pelleted by ultracentrifugation at 314,000*g*(max) for 45 min at 6°C. The resulting pellet was briefly rinsed with Buffer D (pH 7.1), subjected to another ultracentrifugation, and then thoroughly resuspended by gentle mixing in a minimal volume (60–90 µl) of Buffer D (pH 7.1) + 25% Glycerol. Samples were stored on ice prior to spectroscopic analysis.

EPR spectroscopy A typical EPR sample contained V_f= 14.25 µl and consisted of the following: 12.71 or 13.25 µl spin labeled mutant proteoliposomes (43–95 nmoles); 0.5 or 1.04 µl H_2O *versus* 100 mM citrate (C_f) *versus* 15 mM PLP (C_f); and 0.5 µl DMSO *versus* varying concentrations of inhibitor 792949. Aqueous solutions were stored on ice, while organic reagents were stored at room temperature. The order of reactant addition to the proteoliposomes was first aqueous then second organic reagent. All reactions were assembled, with thorough gentle mixing after each addition of reactant to the proteoliposomes, immediately before scanning.

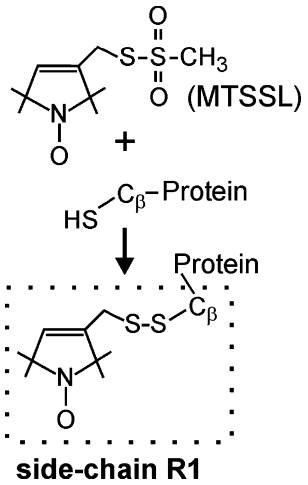

Fig. 1 Site-directed spin labeling reaction. This figure depicts the reaction of a single-Cys CTP mutant with the spin label MTSSL to generate a side-chain denoted as R1

All samples were loaded into round borosilicate capillary tubes of dimension 0.6 mm · 0.84 mm · 75 mm (i.d. · o.d. · length, VitroCom, Mt. Lakes, NJ). EPR spectra were obtained on a Bruker EleXsys 580 spectrometer using a Bruker High Sensitivity resonator at room temperature. All spectra were recorded at 2 milliwatt incident microwave power using a field modulation of 1.0–1.5 Gauss at 100 kilohertz. In order to quantify the spectral changes of R1 residues in CTP that are caused by ligand binding, the root-mean-square (RMS) value for each pair of compared spectra were calculated. Briefly, the EPR spectra obtained in the presence and absence of the ligand were normalized to the same area (area of 1) by double integration using the Bruker Xepr program, with baseline corrections before each integration step. The difference spectrum was then calculated using the normalized spectra. The power spectrum of the difference spectrum was then obtained by squaring the amplitude of the difference spectrum. The area of this power spectrum was calculated by integration. This area was divided by the 100 Gauss scan and the square root of the resulting value was designated as RMS.

Miscellaneous SDS-PAGE was conducted using a precast 14% Tris-glycine gel and protein was visualized with Coomassie Blue according to the manufacturer's (Invitrogen) instructions. Protein was quantified utilizing the Amido Black method of Kaplan and Pedersen (1985).

Results

In the present investigation, we used the site-directed spin labeling method of EPR spectroscopy (Hubbell et al. 1998,

2000; Feix and Klug 1998; Columbus and Hubbell 2002; Klug and Feix 2008; Klare and Steinhoff 2009) to explore the effect of substrate and inhibitors on the conformation of the yeast mitochondrial CTP. Previously, we have shown that the CTP contains two substrate (i.e., citrate) binding sites that reside at increasing depths within the membrane bilayer. These sites are depicted in Fig. 2 with amino acid side-chains of *site 1* residues denoted as magenta stick figures and the side-chains of *site 2* residues as orange stick figures. In the present investigations we chose to study single-Cys residue locations, depicted in Fig. 2 as cyan spheres, that reside sufficiently close to a given binding site to enable its reporting on that environment, but not so close such that the mutation would be disruptive of binding site function. We have previously demonstrated (Kaplan et al. 2000a; Ma et al. 2005, 2007) that Cys mutations placed at each of these locations did not substantially alter CTP function. With this idea in mind, residue locations 183 and 187 (located in TMD IV) were chosen to report on binding *site 1*, residue location 39 on binding *site 2*, and residue 179 on both *sites 1 and 2*. In order to test the idea that substrate or inhibitor binding might cause long-range conformational changes within the CTP, we also studied location 47, which is located in the matrix-facing loop A, and residue location 118 which is thought to reside near the monomer-monomer interface in the homodimer (Ma et al. 2005).

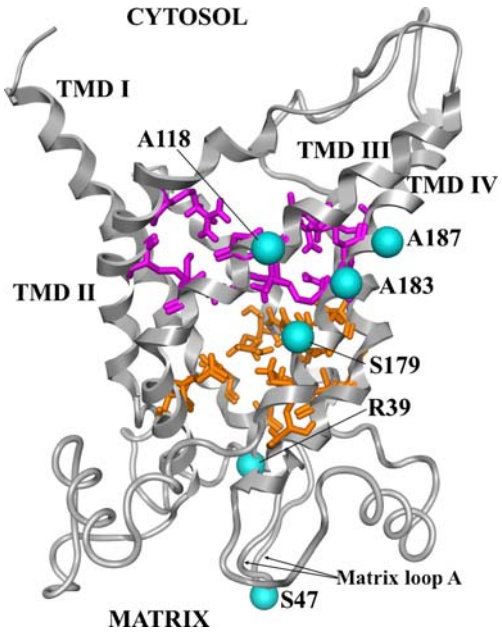

Fig. 2 Model of the CTP showing the substrate binding sites and the locations of spin labels. The backbone of the protein is shown as a gray ribbon. Spin labeled residues are shown as cyan spheres at the alpha-carbon positions. Substrate binding site 1 residues (within 4.5 Å of citrate) are shown as magenta stick structures, and substrate binding site 2 residues are shown as orange stick structures. Matrix loop A (containing S47) and transmembrane domain helices I - IV and are labeled

As depicted in Panels A and B of Figs. 4 and 5, R1 located at all positions except 118, displayed a spectral lineshape characteristic of relatively rapid tumbling motion of the spin label which is typically observed on either solvent-exposed helical surfaces or loops in which R1 residue motion is not limited by tertiary contact with other portions of the protein. These spectra were consistent with the locations proposed in our CTP homology model depicted in Fig. 2. In contrast, residue 118 displays a spectrum that is characteristic of a relatively slow tumbling motion which is typically observed at sites that exhibit significant tertiary contact with other residues such as would be observed at a helix-helix interface or at other domains within the protein interior (Mchaourab et al. 1996; Langen et al. 2000). We note that the observed lineshape for 118 is consistent with our earlier prediction (Ma et al. 2005) that Ala118 may reside near the monomer-monomer interface in homodimeric CTP.

In the present studies we compared the effects of citrate (the native substrate) and three CTP inhibitors (i.e., BTC, compound 792949, and PLP) on the EPR spectra of each of the six spin-labeled CTP variants. For comparative purposes, the structure and molecular dimensions of each of these ligands are depicted in Fig. 3. BTC is the classical, defining inhibitor of the CTP (Robinson et al. 1971; Palmieri et al. 1972). It is a mixed inhibitor of the Cys-less CTP with a strong competitive component and a K_{ic}=0.12±0.02 mM (Aluvila et al. 2010). Superposition of the structures of citrate and BTC indicates very similar locations for the three carboxylate groups. BTC is a relatively small molecule (Fig. 3) and is thought to bind sequentially to sites 1 and 2 with its most prominent binding interactions occurring at site 2. In contrast, compound 792949 was recently discovered via *in silico* screening of a database of commercially available compounds followed by experimental testing of selected compounds (Aluvila et al. 2010). It is approximately double the length of BTC (Fig. 3) and is a purely competitive inhibitor of the CTP with a K_{ic}=0.048± 0.007 mM. Docking calculations indicate that it spans and binds to both substrate binding sites simultaneously. Finally, PLP is a lysine-selective covalent modification reagent which in the absence of reducing agent forms a reversible Schiff base (Lundblad 1991). We have previously demonstrated that PLP behaves as a linear mixed inhibitor of the CTP, with a predominantly competitive component and displays a K_{ic} of 3.6±0.8 mM (Remani et al. 2008). PLP exerts its main inhibitory effect via binding to Lys-83 in binding site 1, and a small effect via binding to residues Lys-37 and Lys-239 in site 2.

Figure 4 depicts the mobility change in the spin-labeled side chains induced by both citrate (the native substrate) and the classical inhibitor BTC. As depicted in Panels A &

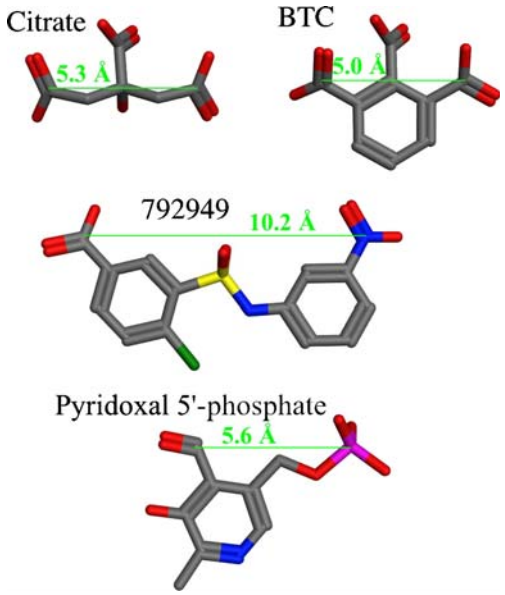

Fig. 3 Structures of citrate, BTC, 792949, and pyridoxal 5′-phosphate. Hydrogens have been omitted for clarity. Gray = carbon, blue = nitrogen, red = oxygen, yellow = sulfur, green = chlorine, pink = phosphorus. Distances were measured between the centers of the atoms shown

C, citrate causes barely detectable spectral changes at each of the positions tested, except with 39R1 CTP where a slight immobilization of the spin-label is observed. As shown in Panels B and C, BTC causes somewhat more spin label immobilization with 179R1, 183R1, 187R1, and 39R1. The largest effect was observed at position 183.

We next measured the effects of the inhibitory compounds PLP and 792949 on CTP conformation by acquiring EPR spectra of the spin-labeled CTP residues in the presence and absence of a given inhibitor. The effects of these inhibitors on EPR spectra are depicted in Fig. 5 Panels A and B. It should be noted that in this figure only a 20 Gauss portion of the entire 100 Gauss scan is depicted. This portion of the spectrum known as the "low-field hyperfine line" is the region in which the mobile and immobile components of the EPR spectrum are most clearly resolved (Budil et al. 1996; Barnes et al. 1999; DeSensi et al. 2008). As depicted in Fig. 5, Panel A at most residues 15 mM PLP caused significant changes in the EPR spectra which were indicative of immobilization of the spin-label. These changes consist of a decrease in the amplitude of the EPR spectrum in the region corresponding to the mobile spin-label population (denoted as **m** in Fig. 5) and a concurrent increase in the amplitude of the spectrum in the region corresponding to a less mobile (i.e., immobile) population of the spin-label (denoted as **i**). The spectral changes caused by inhibitor were quantified by the root-mean-square (RMS) of the amplitude changes between a spectrum obtained in the presence of a given inhibitor compared to a control spectrum obtained in its absence. The RMS parameter is calculated using the entire 100 Gauss spectrum (see Experimental Procedures) and is depicted in Panel C. Two points are noteworthy. *First,* at all positions PLP causes significantly greater immobilization than did either BTC or citrate (compare Panel C in Figs. 4 and 5). *Second,* based on RMS values, the rank order of immobilization is 183R1 >187R1 > 179R1 > 39R1 > 47R1 > 118R1.

The effects of compound 792949 on spin-label mobility are depicted in Fig. 5 Panels B and C. Importantly, 15 mM

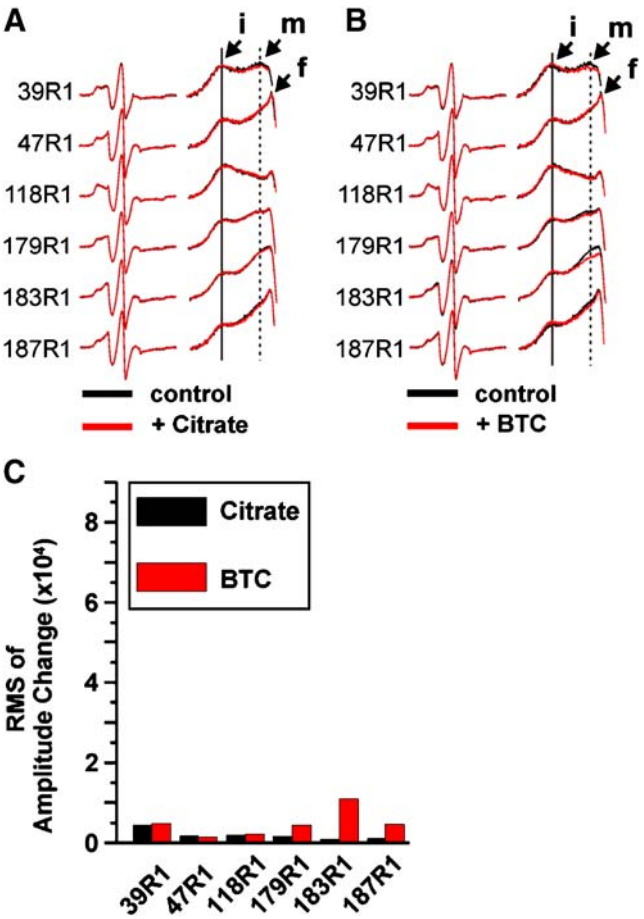

Fig. 4 Conformational changes in CTP caused by extra-liposomal citrate *versus* BTC. **Panel A***:* Superimposed EPR spectra in the presence (*red trace*) and absence (*black trace*) of 20 mM citrate (30 mM for 118R1) obtained with CTP spin-labeled at the residue locations indicated and reconstituted into proteoliposomal vesicles. To the right is an enlargement of the low field hyperfine line corresponding to a 20 Gauss window of the spectra. The immobile and mobile components are denoted as **i** and **m** (indicated by the solid and dotted vertical lines), respectively; **f**, denotes the presence of small quantities of free spin-label. All spectra (100 Gauss scan) were normalized to the same area by double integration. **Panel B***:* Superimposed EPR spectra in the presence (*red trace*) and absence (*black trace*) of 20 mM BTC (30 mM for 118R1). **Panel C***:* Spectral changes caused by ligand relative to each control, as depicted in Panels A and B, were quantified as the root-mean-square (i.e., RMS) of the amplitude change of the entire 100 Gauss scan, as described in "Experimental Procedures"

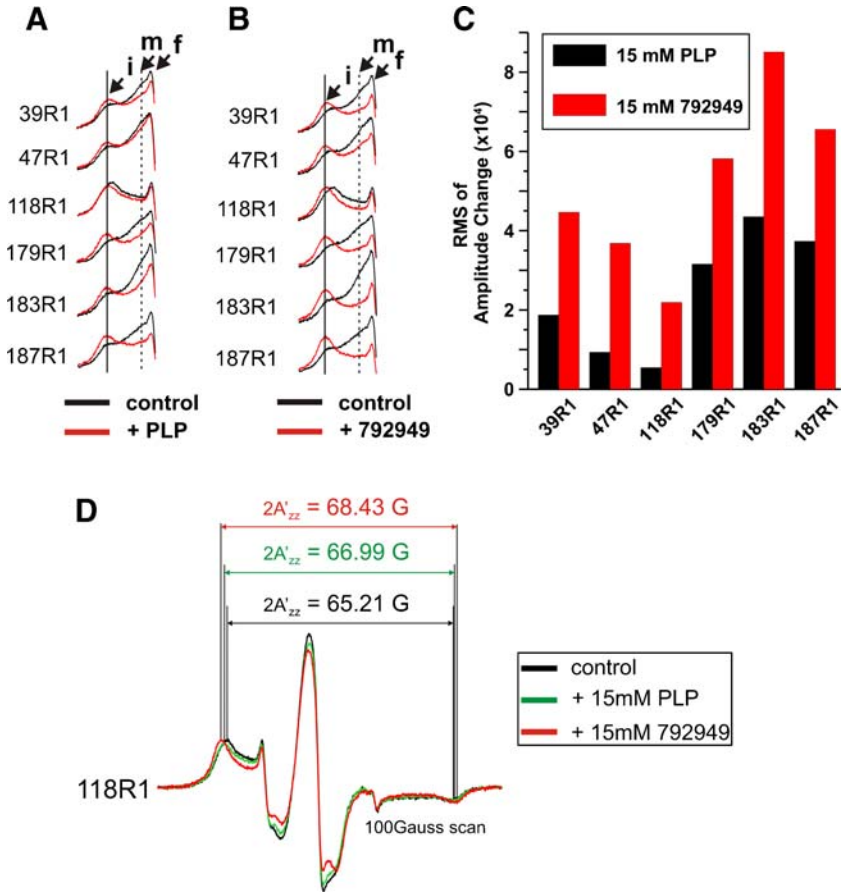

Fig. 5 Conformational changes in CTP caused by *extra-liposomal* PLP *versus* compound 792949. **Panel A***:* An enlargement of the low field hyperfine lines corresponding to a 20 Gauss window of superimposed EPR spectra in the presence (*red trace*) and absence (*black trace*) of 15 mM PLP is depicted. All of the original spectra (100 Gauss scan) were obtained using reconstituted CTP spin-labeled at the residue locations indicated and were normalized to the same area by double integration. The immobile and mobile components are denoted as **i** and **m** (indicated by the solid and dotted vertical lines), respectively; **f**, denotes the presence of small quantities of free spin-label. **Panel B***:* The same low field portion of the EPR spectra obtained in the presence (red trace) and absence (black trace) of 15 mM compound 792949 is depicted. **Panel C***:* Spectral changes caused by ligand relative to each control, were quantified as the RMS of the amplitude change of the spectra in the entire 100 Gauss scan. **Panel D***:* The EPR spectral parameter $2A'_{zz}$ was measured from the entire spectra for 118R1 in the absence and presence of inhibitors. The spectra and the $2A'_{zz}$ values are color-coded as depicted

792949 causes significantly greater immobilization than observed with either PLP or BTC at each spin-labeled residue. Furthermore, the rank order of immobilization is the same as observed with PLP. Interestingly, we note that the subset of spin-labeled residues that report most directly on CTP substrate binding sites (i.e., residues 183, 187, 179, and 39) display the greatest extent of spin-label immobilization upon binding any of the three inhibitors tested. At the six sites tested, the immobilization effect due to 15 mM external 792949, as quantified by the RMS value, was on average approximately double the extent of immobilization that was observed with 15 mM PLP, and approximately 10 times greater than the immobilization observed with 20–30 mM BTC.

Of note, residue 118R1 displayed a relatively immobile lineshape even in the absence of inhibitor. Consequently, inhibitor-induced spectral changes do not result in large amplitude changes and hence RMS values are relatively small. However, despite this small change in RMS, an EPR spectral parameter known as $2A'_{zz}$ (Fig. 5d) significantly increases upon addition of either PLP or 792949, thereby indicating that these inhibitors cause further immobilization of spin-label at this location, as well as the other sites mentioned above.

Next, we investigated the effect of the *vectorial* addition of compound 792949 on the lineshape of 179R1. Figure 6, Panel A depicts the entire EPR spectra obtained following the inclusion of ligand in the *intra-* and/or the *extra-liposomal* compartments. Panel B depicts an enlargement of the low-field hyperfine line, and Panel C depicts the RMS values, thereby providing a quantification of the spectral changes that occurred due to the inclusion of ligand in a given compartment(s). We observed that, upon addition of external citrate (gold trace), little change in the EPR spectra occurs compared to the control (black trace). In sharp contrast, addition of 10 mM compound 792949 to the

extra-liposomal compartment causes a large decrease in the mobile population and a concurrent increase in the immobile population of the spin label (blue trace in Panels A and B). In contrast, upon inclusion of 10 mM *intra-liposomal* 792949, we observe only a small decrease in the mobile component of the spectrum and little change in the immobile component (green trace). Importantly, this observation suggests that binding of 792949 to CTP from the internal surface of the proteoliposomes (i.e., to the *matrix-facing* conformation) occurs to a much lesser extent than does binding to the CTP from the external surface (i.e., the *cytosolic-facing* conformation). Upon inclusion of compound 792949 in both the *intra-* and the *extra-liposomal* compartments (red trace) the spectral changes observed were approximately additive relative to the changes observed when the inhibitor was included in each compartment individually. The implications of these key observations, namely the absence of a substantial effect of 792949 from the internal surface and its strongly immobilizing effect from the external surface, will be discussed below.

Figure 7, Panels A-C demonstrate the effects of the vectorial addition of PLP on the EPR spectra. We observed

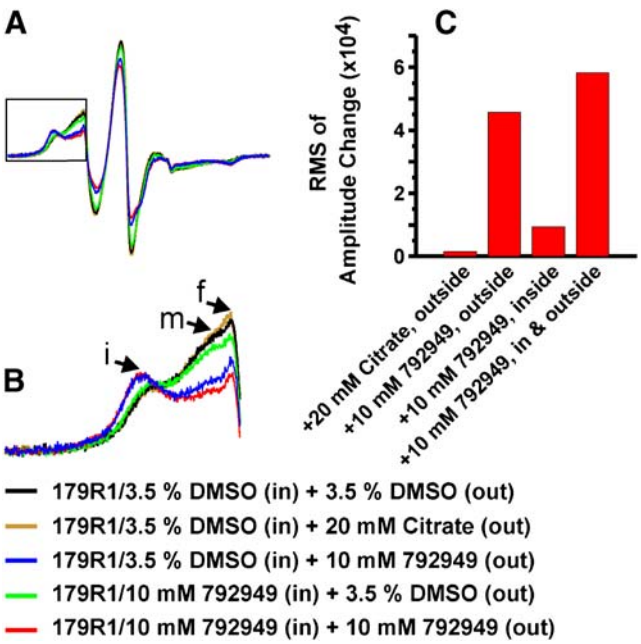

Fig. 6 Conformational changes in CTP caused by *intra-liposomal* versus *extra-liposomal* placement of compound 792949. **Panel A**: The superposition of 5 different EPR spectra obtained with 179R1 CTP reconstituted in liposomes. The presence and absence of various internal and external ligands are color-coded as indicated in the figure. **Panel B**: An expansion of the boxed area in *Panel A* corresponding to the low field region of the spectra, detailing the change in the immobile (**i**) and mobile (**m**) populations in the EPR spectra. The presence of a small, contaminating amount of free spin-label is denoted by **f**. **Panel C**: Quantitation of spectral change by the RMS value of the amplitude change of each spectrum relative to the condition in the absence of ligand (black trace in A)

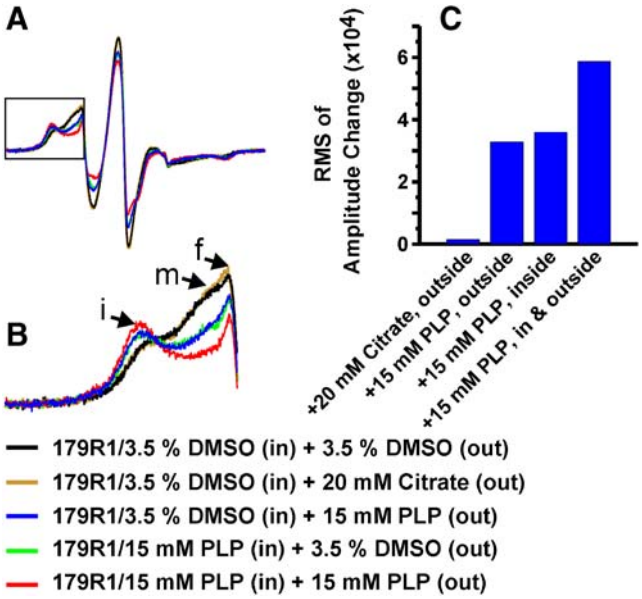

Fig. 7 Conformational changes in CTP caused by *intra-liposomal* versus *extra-liposomal* placement of PLP. **Panel A**: The superposition of 5 different EPR spectra obtained with 179R1 CTP reconstituted in liposomes. The presence and absence of various internal and external ligands are color-coded as indicated in the figure. **Panel B**: An expansion of the boxed area in *Panel A* corresponding to the low field region of the spectra, detailing the change in the immobile (**i**) and mobile (**m**) populations in the EPR spectra. The presence of a small, contaminating amount of free spin-label is denoted by **f**. **Panel C:** Quantitation of spectral change by the RMS value of the amplitude change of each spectrum relative to the condition in the absence of ligand (black trace in A)

that upon addition of either *extra-* or *intra-liposomal* PLP, a similar increase in the immobile component and decrease in the mobile component of the EPR spectra occurs (i.e., compare the blue and green traces in Panel B to the control black trace). Furthermore, the effect is approximately additive when PLP is added to both compartments. Thus, in sharp contrast to compound 792949, PLP is able to effectively bind to the CTP from the *intra-liposomal* surface. Relatedly, *external* 792949 more potently locks the CTP into an immobile conformation than does *external* PLP.

Discussion

The objective of the present investigation was to explore the effects of substrate and inhibitors on the conformation of the yeast mitochondrial CTP using the site-directed spin labeling approach of EPR spectroscopy. It is noteworthy that the EPR spectra observed at each of the six locations were consistent with the topological locations predicted by the CTP homology-modeled structure (Walters and Kaplan 2004) and our proposed monomer-monomer interface in homodimeric CTP (Ma et al. 2005), thereby providing new

validation for these models. Furthermore, several key novel findings were obtained by our studies. *First,* we demonstrate that citrate, the native substrate, does not cause any significant change in the spectra of spin label residing at multiple locations throughout the CTP, thus indicating that citrate binding to the CTP substrate binding sites does not alter the dynamics of the side-chains and the backbone of the CTP in the non-binding site regions of the transporter in a global manner. This finding is consistent with our expectation that in both the absence and presence of substrate the CTP displays the flexibility required of a membrane transport protein. *Second,* each of the three inhibitors tested (Fig. 3), caused spectral changes that indicate varying degrees of immobilization of the spin label (Figs. 4 and 5). Thus inhibitor binding appears to reduce CTP flexibility, perhaps locking it into one of the conformation(s) that is normally assumed during the transport cycle. The latter point is supported by our earlier findings that each of the inhibitors tested display a strong competitive component in their inhibition mechanism (Remani et al. 2008; Aluvila et al. 2010).

Experiments conducted with *external* compound 792949 (Fig. 5, Panels B & C), a purely competitive inhibitor that is capable of spanning binding sites 1 and 2 (Aluvila et al. 2010), yielded EPR spectra that indicate a concurrent substantial increase in the immobile component and decrease in the mobile component at each of the six locations tested, indicating that the effect is global. It is noteworthy that 792949 caused considerably greater immobilization than did BTC (compare Panel C in Figs. 4 and 5). These findings support the conclusion that the binding of compound 792949 causes a shift in the conformational equilibrium such that the side chain R1 in CTP becomes less mobile. The inhibitor-induced decrease in mobility could originate from increased tertiary interactions of R1 with nearby CTP domains and/or from a reduction in the CTP backbone motion (Columbus and Hubbell 2002), either of which signifies a more locked, rigid CTP conformation. Relatedly, we note that as depicted in Fig. 3, an important difference between compound 792949 and either BTC or citrate is that the former has a length sufficient to span both substrate binding sites within the CTP, whereas BTC and citrate do not. We posit that it is these additional specific binding interactions of 792949 to both CTP substrate binding sites simultaneously (Aluvila et al. 2010) that impose significantly more restriction on CTP mobility than observed with either BTC or citrate.

We also studied the effect of *extra-liposomal* PLP, a lysine-selective reagent that has been shown to inhibit the CTP, on the EPR spectrum. We observed that PLP causes significant immobilization of spin-label placed at six different locations within the CTP (Fig. 5). We note that the immobilizing effect by *external* PLP is less potent than observed with external 792949, but is more pronounced than observed with BTC or citrate. Consequently, we posit that external PLP causes an intermediate degree of locking of the CTP conformation, a finding that is consistent with our previous observation that PLP inhibits the CTP mainly via interactions of residue Lys83 in substrate binding site 1 and is of insufficient length to simultaneously span sites 1 and 2 in their entirety.

Our investigations into the *vectorial* effect of the inhibitors compound 792949 and PLP on the lineshape of 179R1 (Figs. 6 and 7) provide important clues regarding CTP function. For example, the finding that only upon addition of compound 792949 from the *external* surface of the proteoliposomes do we observe substantial changes in the EPR spectra suggests that binding of 792949 to CTP from the *internal* surface of the proteoliposomes occurs to a much lesser extent than does binding to the CTP from the *external* surface. These data strongly support the conclusion that: i) in our proteoliposomal preparation the CTP is predominantly incorporated into the liposomal bilayer asymmetrically (i.e., unidirectionally; *cytosolic-facing* conformation oriented outwards); and ii) in the *cytosolic-facing* conformation of the CTP, substrate binding sites 1 and 2 are primarily accessible to the extra-liposomal surface. Furthermore, it is noteworthy that previously we hypothesized, based on the facts that 792949 was identified via docking experiments using the *cytosolic-facing* conformation of the CTP as the template and based on kinetic data, that 792949 binds exclusively to the *cytosolic-facing* conformation of the CTP (Aluvila et al. 2010). Our present findings on the vectorial effect of 792949 on EPR spectra provide additional support for this conclusion. Finally, if CTP functions as a homodimer (Kotaria et al. 1999), our data with compound 792949 suggest that the conformational changes in each of the two monomers are tightly coordinated. Thus upon addition of 792949, the locking of one monomer's conformation results in a similar locking of the other's, thereby reducing spin-label mobility at both locations within the CTP and resulting in a highly immobilized spectrum.

Interestingly, we observed that *intra-liposomal* PLP caused considerably more immobilization of the spin labels than did *intra-liposomal* compound 792949. Moreover, in the case of PLP we observed a similar extent of immobilization when the inhibitor was added to either the *intra-* or the *extra-liposomal* compartments. Furthermore, the effect is approximately additive when PLP is added to both compartments. This is in sharp contrast to compound 792949, which exerts nearly its entire effect from the *extra-liposomal* surface. These observations beg the question as to how PLP can interact with and immobilize the CTP from its *intra-liposomal* surface, whereas compound 792949 cannot. We note several points. *First,* as depicted in Fig. 8, in the *cytosolic-facing* conformation of the CTP,

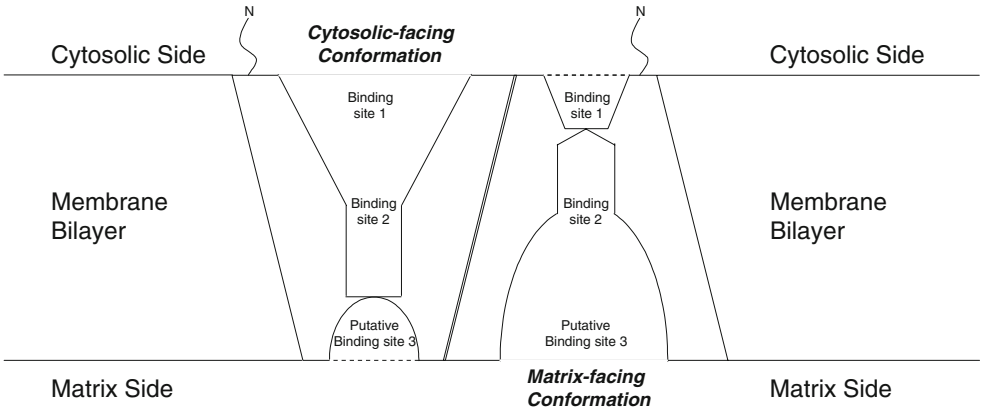

Fig. 8 Schematic representation of substrate binding sites within homodimeric CTP located within the mitochondrial inner membrane bilayer. Binding sites 1 and 2 and a hypothetical binding site 3 are depicted in the *cytosolic-facing* and *matrix-facing* conformations of each monomer comprising the CTP homodimer. Each of the monomers in the homodimer consists of six TMDs which reside in the bilayer in the same orientation with their N-termini exposed to the cytosolic side. Binding site architecture and accessibility differ in the two conformations depicted. Dashed lines indicate questionable accessibility between a given substrate binding site and the aqueous milieu

which was used to identify compound 792949 via *in silico* docking, the translocation pathway may be closed near the matrix surface (denoted as a dotted line). Thus, it is not surprising that the inhibitor is unable to bind to the *cytosolic-facing* conformation from its internal surface. Furthermore, the minimal change in the EPR spectrum caused by *intra-liposomal* 792949 suggests that this inhibitor does not bind significantly to the other CTP monomer that exists in the *matrix-facing* conformation within the homodimer. **Second,** with regard to PLP we note that the CTP contains numerous lysines both near the matrix surface as well as within the translocation pathway. Furthermore, we previously demonstrated that most (i.e., 78%) of the inhibition of transport caused by *extra-liposomal* PLP arises from its binding to Lys-83 in binding site 1, whereas the remaining inhibition originates from PLP binding to site 2 residues Lys-37 and/or Lys-239. Presumably, the immobilization of the EPR spectra caused by external PLP is mediated via binding to these same residues. The question then arises as to the mechanism by which *intra-liposomal* PLP causes the observed spectral changes. We note that in the CTP homodimer the *cytosolic-facing* and the *matrix-facing* conformations will always exist in equal measure. As depicted in Fig. 8, we postulate that in the *cytosolic-facing* conformation, binding site 1 is accessible to the external aqueous milieu but not the internal aqueous compartment. Furthermore, we propose that in the *matrix-facing* conformation, CTP binding site 1 exists in a different conformation that may or may not remain accessible to the *external* milieu (Aluvila et al. 2010), as indicated by the dotted line in the figure and is not extensively accessible to *internal* PLP. Thus, we propose that the *intra-liposomal* PLP effect is due either to a more pronounced effect on binding site 2 lysines in this *matrix-facing* conformation and/or to the binding of PLP to other internal lysines. With respect to the latter idea, we note that conserved lysines exist within CTP domains that are located near the internal surface of the bilayer. We postulate that these residues may participate in the formation of a third substrate binding site in the *matrix-facing* conformation of the CTP and that the additional immobilization caused by *intra-liposomal* PLP may arise via binding to this hypothetical third site. Finally, we note that at the concentrations tested (i.e., 15 mM PLP and 10 mM compound 792949), the total extent of immobilization achieved in the presence of *intra-* plus *extra-liposomal* inhibitor is similar for both PLP and compound 792949. Significantly, the ability of these two inhibitors to lock domains within the CTP to different extents depending on the site of their addition, will provide complementary, yet overlapping means for probing CTP architecture.

Our findings with spin label placed at six different locations within the CTP indicate that inhibitor binding causes global conformational changes that result in the immobilization of the spin label at each location tested. Moreover, we note that, with each of the three inhibitors tested, based on RMS values, we see the same pattern of residue-dependent extent of immobilization (i.e., 183R1 > 187R1 >179R1 > 39R1 > 47R1 > 118R1). For example, with a given ligand, TMD IV residues 179R1, 183R1, and 187R1, which are located on the same face of this helix, all exhibit greater extents of immobilization than are observed at the other locations tested. This result strongly suggests that immobilization of these spin labels is due to a rigid body motion of the TMD IV helix which arises from inhibitor binding to CTP substrate binding sites 1 and/or 2. One can envision that this motion might be either a twisting of the helix that results in the placement of the TMD IV spin labels near the surface of an adjacent helix and/or by translation of the TMD IV helix toward the central axis of

the CTP transport pathway thereby causing a decrease in the distance between CTP TMD helices forming new spin label side chain interactions that restrict motion. With respect to 39R1 we note that it is located near the matrix end of TMD I, likely points towards the matrix compartment, and is in close proximity to binding site 2 and thus reports on conformational changes at this site. Similar to most of the other residues examined, its EPR spectra exhibited an intermediate mobility in the absence of inhibitor (Figs. 4 and 5). As observed with the other residues, binding of externally added inhibitor results in a large increase in the immobile population and a concurrent decrease in the mobile population of spin label at this location. Thus, this domain also becomes less flexible for the reasons described above. Finally, we note that the four locations (i.e., 39, 179, 183, 187) that report most directly on substrate binding sites 1 and/or 2, display the greatest changes in the EPR spectrum upon addition of inhibitor.

Two additional locations were studied (i.e. 47R1 and 118R1) which are not located near substrate binding sites 1 or 2. We note that 47R1 is located in Matrix Loop A which connects TMDs I and II (see Fig. 2), and displays a mobility comparable to that of R1 located on TMD IV (ie., at locations 179, 183, and 187) in the absence of inhibitor. This finding suggests that either this loop is partially structured and/or unlike the depiction in Fig. 2, it may in fact have substantive tertiary interactions with other nearby domains that limit its mobility. In the presence of inhibitors, its mobility also is reduced suggesting long-range conformational communication between the inhibitor binding sites and this domain.

Previously, based on both kinetic analysis and molecular modeling (Ma et al. 2005) we hypothesized that residue 118 resides near the monomer-monomer interface in the homodimer and may be involved in coordinating the conformational change between the two monomers. Interestingly, we note that despite the fact that the side chain of residue 118 points away from the CTP monomer in the direction of the lipid bilayer, 118R1 nonetheless displays a very immobilized EPR spectra, indicating considerable tertiary contact at this location. In the presence of CTP inhibitors, its mobility is further diminished (Fig. 5) supporting the notion that conformational communication may occur between the substrate binding sites and the monomer-monomer interface in homodimeric CTP.

Relatedly, the following note of caution is in order. The molecular interpretations that we have posited to account for the observed EPR data are based in part on our homology-modeled structure of the CTP (Walters and Kaplan 2004) which, as mentioned above, was developed from the crystallographic structure of the mitochondrial ADP/ATP carrier (Pebay-Peyroula et al. 2003). Consequently, the validity of these interpretations relies upon the accuracy of the CTP homology model. We have a high degree of confidence in the correctness of this model since it has accurately predicted the composition of the CTP substrate translocation pathway and the substrate binding sites, as well as a specific steric interaction between Gln182 in TMD IV and Leu120 in TMD III, all of which have been experimentally verified (Kaplan et al. 2000a; Ma et al. 2004, 2005, 2006, 2007). Nonetheless, a high-resolution 3-dimensional crystal structure of the CTP will be needed to unequivocally confirm the validity of certain of the molecular explanations posited for the present findings.

Finally, a critical conclusion derived from these experiments, is that at each of the six sites examined, which reside in vastly different CTP domains, inhibitor binding results in long-range conformational changes as evidenced by changes in EPR spectra. These results support the hypothesis that transport of CTP substrates occurs via a long-range coordinated motion between domains within this carrier. Our future experiments will be directed toward understanding the nature of these conformational changes and the composition of the monomer-monomer interface by directly measuring distances between CTP domains, in the presence and absence of various ligands. Furthermore, the discovery of inhibitors that lock CTP into an immobilized conformation(s), which may represent one or more of the conformations that CTP assumes during its transport cycle, may provide key tools in the search for conditions that yield well-diffracting CTP crystals and thereby pave the way for an atomic resolution structure of the CTP.

Acknowledgments We thank Dr. D.H.T. Harrison for insightful discussions and for critical reading and comments on the manuscript.

We acknowledge the use of the instrumentation and gratefully appreciate the support of the Rosalind Franklin University of Medicine and Science EPR Center.

References

Aluvila S, Sun J, Harrison DHT, Walters DE, Kaplan RS (2010) Mol Pharm 77:26–34

Barnes JP, Liang Z, Mchaourab HS, Freed JH, Hubbell WL (1999) Biophys J 76:3298–3306

Berliner LJ, Grunwald J, Hankovszky HO, Hideg K (1982) Anal Biochem 119:450–455

Brunengraber H, Lowenstein JM (1973) FEBS Lett 36:130–132

Budil DE, Lee S, Saxena S, Freed JH (1996) J Magn Resn. A 120:155–189

Columbus L, Hubbell WL (2002) Trends Biochem Sci 27:288–295

Conover TE (1987) Trends Biochem Sci 12:88–89

DeSensi SC, Rangel DP, Beth AH, Lybrand TP, Hustedt EJ (2008) Biophys J 94:3798–3809

Endemann G, Goetz PG, Edmond J, Brunengraber H (1982) J Biol Chem 257:3434–3440

Feix JB, Klug CS (1998) In: Berliner LJ (ed) Biological magnetic resonance, vol. 14, Spin labeling: The next millennium. Plenum Press, New York, pp 251–281

Heisterkamp N, Mulder MP, Langeveld A, Hoeve JT, Wang Z, Roe BA, Groffen J (1995) Genomics 29:451–456
Hubbell WL, Gross A, Langen R, Lietzow MA (1998) Curr Opin Struct Biol 8:649–656
Hubbell WL, Cafiso DS, Altenbach C (2000) Nat Struct Biol 7:735–739
Jensen MV, Joseph JW, Ronnebaum SM, Burgess SC, Sherry AD, Newgard CB (2008) Am J Physiol Endocrinol Metab 295: E1287–E1297
Joseph JW, Jensen MV, Ilkayeva O, Palmieri F, Alarcon C, Rhodes CJ, Newgard CB (2006) J Biol Chem 281:35624–35632
Kaplan RS, Pedersen PL (1985) Anal Biochem 150:97–104
Kaplan RS, Morris HP, Coleman PS (1982) Cancer Res 42:4399–4407
Kaplan RS, Mayor JA, Johnston N, Oliveira DL (1990a) J Biol Chem 265:13379–13385
Kaplan RS, Oliveira DL, Wilson GL (1990b) Arch Biochem Biophys 280:181–191
Kaplan RS, Mayor JA, Wood DO (1993) J Biol Chem 268:13682–13690
Kaplan RS, Mayor JA, Gremse DA, Wood DO (1995) J Biol Chem 270:4108–4114
Kaplan RS, Mayor JA, Brauer D, Kotaria R, Walters DE, Dean AM (2000a) J Biol Chem 275:12009–12016
Kaplan RS, Mayor JA, Kotaria R, Walters DE, Mchaourab HS (2000b) Biochemistry 39:9157–9163
Klare JP, Steinhoff H-J (2009) Photosynth Res 102:377–390
Klug CS, Feix JB (2008) Methods and applications of site-directed spin labeling EPR spectroscopy. In: Correia JJ, Detrich HW (eds) Methods in cell biology. Biophysical tools for biologists, volume one: in vitro techniques. Academic Press, New York, pp 617–658
Kotaria R, Mayor JA, Walters DE, Kaplan RS (1999) J Bioenerg Biomemb 31:543–549
Langen R, Oh KJ, Cascio D, Hubbell WL (2000) Biochemistry 39:8396–8405
Lundblad RL (1991) Chemical reagents for protein modification. CRC, Boca Raton
Ma C, Kotaria R, Mayor JA, Eriks LR, Dean AM, Walters DE, Kaplan RS (2004) J Biol Chem 279:1533–1540
Ma C, Kotaria R, Mayor JA, Remani S, Walters DE, Kaplan RS (2005) J Biol Chem 280:2331–2340
Ma C, Remani S, Kotaria R, Mayor JA, Walters DE, Kaplan RS (2006) Biochim Biophys Acta 1757:1271–1276
Ma C, Remani S, Sun J, Kotaria R, Mayor JA, Walters DE, Kaplan RS (2007) J Biol Chem 282:17210–17220
Mchaourab HS, Lietzow MA, Hideg MA, Hubbell WL (1996) Biochemistry 35:7692–7704
Palmieri F, Stipani I, Quagliariello E, Klingenberg M (1972) Eur J Biochem 26:587–594
Pebay-Peyroula E, Dahout-Gonzalez C, Kahn R, Trézéguet V, Lauquin GJ, Brandolin G (2003) Nature 426:39–44
Remani S, Sun J, Kotaria R, Mayor JA, Brownlee JM, Harrison DHT, Walters DE, Kaplan RS (2008) J Bioenerg Biomembr 40:577–585
Robinson BH, Williams GR, Halperin ML, Leznoff CC (1971) J Biol Chem 246:5280–5286
Walters DE, Kaplan RS (2004) Biophys J 87:907–911
Watson JA, Lowenstein JM (1970) J Biol Chem 245:5993–6002
Xu Y, Mayor JA, Gremse D, Wood DO, Kaplan RS (1995) Biochem Biophys Res Commun 207:783–789
Xu Y, Kakhniashvili DA, Gremse DA, Wood DO, Mayor JA, Walters DE, Kaplan RS (2000) J Biol Chem 275:7117–7124

This work was supported by National Institutes of Health Grant GM-054642 to R.S.K.